MODELING THE ANISOTROPIC DEFORMATION AND DELAMINATION IN LAMINATED PAPERBOARD

Y. Li, J.-W. Simon and S. Reese

Institute of Applied Mechanics, RWTH Aachen University, Mies-van-der-Rohe Str. 1, D-52074 Aachen, Germany (yujun.li@rwth-aachen.de, www.ifam.rwth-aachen.de)

Keywords: Laminated paperboard, Elastic-plastic, Delamination, Cohesive zone model

ABSTRACT

Laminated paperboard is widely used in packaging products. It generally exhibits highly anisotropic and nonlinear mechanical behavior. The aim of this study is to describe the inelastic material behavior of paper sheet with an orthotropic elastic-plastic model and characterize the interface delamination phenomenon with a cohesive zone model. To this end, a structural tensor-based approach was applied to model the elastic deformation, while a multi-surface based yield criterion was adopted to describe the yield behavior of paper sheet. The model was derived from a thermodynamic framework and was based on the multiplicative split of the deformation gradient in the context of hyperelasticity. The model considered both material densification and internal friction effects, which were observed experimentally. With the material parameters calibrated from a set of simple uniaxial tests in various directions, the model was shown to predict the stress-strain behavior for other orientations satisfactorily. The model was further validated with experiments under complex loading conditions and found to capture the highly anisotropic, elastic-plastic behavior accurately. Furthermore, in order to predict the interface fracture behavior of paperboard, a potential based cohesive zone model (CZM) in a phenomenological way was proposed to include the fiber bridging effect. The cohesive energy potential was constructed using an exponential function, and the cohesive traction-separation relationships were obtained from the gradient of the potential. The proposed model was evaluated by simulating the double cantilever beam (DCB), end-notched flexure (ENF), and mixed mode tests. The results agree well with experimental data. Finally, the proposed elastic-plastic model for paper sheet and the CZM model for the interface were used to study the paperboard creasing process.

1 INTRODUCTION

Laminated paperboard is one of the most common packaging materials in industry due to its beneficial characteristics, such as low price, sustainability, and recyclability. Depending on the specific requirement, it can be easily designed as a single layer paper or multi-layer sandwich structure. This material exhibits a highly anisotropic mechanical behavior due to its manufacturing process; including anisotropic elasticity, initial yielding, strain hardening, and tensile failure. The principal directions of paper are the machine direction (MD), cross-machine direction (CD), and out-of-plane direction (ZD). Due to the manufacturing process, the magnitude of mechanical properties in MD can be up to five times higher than that in CD, and up to 100 times higher than that in ZD.

In industry, almost all paperboard packaging includes a creasing operation to obtain a locally deformed zone and a subsequent folding or deep drawing process to form the final box. During creasing, the paperboard is pressed into a channel by a creasing rule to introduce delamination to locally reduce its bending stiffness. In the folding process, the outer layers of paperboard are loaded in-plane tension while the inner layers are in compression. The deformation in deep drawing processes is even more complex, which usually introduces positive longitudinal strain but negative transversal strain. Conclusively, all the operations include a complex loading-unloading-reloading deformation, leading to some common defects such as cracking, buckling, spring-back, and so on. To obtain an accurate prediction of these operations, it is essential to perform studies on two aspects, namely the paper sheet anisotropic behavior and the interface delamination between different layers. In literature, different methods have been developed to model the mechanical deformation of paper sheet, e.g. [1-3], and the interface delamination behavior, e.g. [4-6].

In general, the experimentally observed mechanical behavior of paper includes: (i) elastic-plastic anisotropy, (ii) different yielding between tension and compression, (iii) pressure dependent yielding behavior, (iv) large deformation in the out-of-plane direction, (v) densification effect under out-of-plane compression, and (v) internal friction effect in the out-of-plane direction under combined shear and compression. Additionally, the paperboard delamination tests show a pronounced fiber bridging effect in the wake of the crack tip. All the phenomena should be considered in the construction of the constitutive model in order to predict an accurate deformation under complex loadings. Therefore, in the current work, a general elastic-plastic constitutive model was proposed to incorporate all the characteristics of paper sheet mechanical response, while a potential based cohesive zone model (CZM) was adopted to describe the interface fracture phenomenon.

2 ELASTIC-PLASTIC MODEL OF PAPER SHEET

2.1 Elasticity

According to the studies by Stenberg [1] and Xia et al. [2], it is reasonable to study the in-plane and out-of-plane behavior in an uncoupled way. Therefore, an elastic-plastic model, including an in-plane and an out-of-plane part, is developed to represent all the critical aspects of the mechanical response.

To model the anisotropic elastic response of paper, the elastic part of the free energy is constructed based on the concept of structural tensors, $\mathbf{M}_\alpha = \mathbf{N}_\alpha \otimes \mathbf{N}_\alpha$. It is expressed as

$$\psi^e = \psi^e_{lin}(\mathbf{C}_e, \mathbf{M}_\alpha) + \psi^e_{op}(\mathbf{C}_e, \mathbf{M}_\alpha, \mathbf{C}_p), \tag{1}$$

where the subscripts *lin* and *op* refer to the contributions of the small deformation range and the large out-of-plane deformation, respectively, and $\mathbf{C}_e$ and $\mathbf{C}_p$ denote the elastic and plastic right Cauchy-Green tensor, respectively. The compressibility of paper during plastic deformation is reflected by $J_p = \det \mathbf{C}_p \neq 1$. Unlike most of classical elastic-plastic models, $\mathbf{C}_p$ is present in the elastic energy function in the current model representing the influence of permanent densification on the elastic deformation. Having defined the free energy, the specific form of each function can be developed using the structural tensor based anisotropic model (Reese et al. [7]):

$$\begin{aligned}\psi^e_{lin} = {} & K_2^{\text{iso}}(I_2 - 2I_1 + 3) + K_1^{\text{ani }1}(I_4 - 1)^2 + K_2^{\text{ani }1}(I_5 - 4I_4 + 3) + K_1^{\text{ani }2}(I_6 - 1)^2 \\ & + K_2^{\text{ani }2}(I_7 - 4I_6 + 3) + K^{\text{coup }1}(I_1 - 3)(I_4 - 1) \\ & + K^{\text{coup }2}(I_1 - 3)(I_6 - 1) + K^{\text{coup ani}}(I_4 - 1)(I_6 - 1),\end{aligned} \tag{2}$$

where $K_2^{\text{iso}}, K_1^{\text{ani }1}, K_2^{\text{ani }1}, K_1^{\text{ani }2}, K_2^{\text{ani }2}, K^{\text{coup }1}, K^{\text{coup }2}, K^{\text{coup ani}}$ are material constants which have to be fit to experiments. In addition, the invariants, I_i (i = 1,…,7), are given as

$$\begin{aligned} & I_1 := \text{tr}\mathbf{C}_e, I_2 := \frac{1}{2}\left(I_1{}^2 - \text{tr}\left(\mathbf{C}_e{}^2\right)\right), I_3 := \det\mathbf{C}_e, \\ & I_4 := \text{tr}(\mathbf{C}_e\mathbf{M}_1) = \mathbf{C}_e : \mathbf{M}_1, I_5 := \text{tr}\left(\mathbf{C}_e{}^2\mathbf{M}_1\right) = \mathbf{C}_e{}^2 : \mathbf{M}_1, \\ & I_6 := \text{tr}(\mathbf{C}_e\mathbf{M}_2) = \mathbf{C}_e : \mathbf{M}_2, I_7 := \text{tr}\left(\mathbf{C}_e{}^2\mathbf{M}_2\right) = \mathbf{C}_e{}^2 : \mathbf{M}_2. \end{aligned} \tag{3}$$

To account for the influence of material densification on the nonlinear out-of-plane elastic response, the latter term in (1) is given as follows,

$$\psi^e_{top} = K^{top}\left(1 + J_p^{-\beta}\right)\left[\frac{1}{2}\left(I_8{}^2 - 1\right) + \frac{1}{\alpha}\left(I_8{}^{-\alpha} - 1\right)\right], \tag{4}$$

where $K^{top}$and α are positive elastic material constants. β denotes the densification parameter and is always positive by taking its physical meaning into account. Its lower limit, β = 0, describes a normal hyperelastic behavior without any densification effect. Using the relationship $\sum_{i=1}^{3}\mathbf{M}_i = \mathbf{I}$, the variable I_8 can be expressed in the form

$$I_8 := \text{tr}(\mathbf{C}_e\mathbf{M}_3) = \mathbf{C}_e : \mathbf{M}_3 = I_1 - I_4 - I_6. \tag{5}$$

2.2 Plasticity

The work of Xia et al. [2] is extended to capture the aforementioned plastic behavior in the in-plane and out-of-plane directions. The adopted multi-surface yield function and flow potential are based on the fact that the ratio between lateral plastic strain and axial plastic strain is nearly constant for both MD and CD tension. The experimental evidence has also indicated that the plastic yielding coupling effect between both directions could be neglected in most cases. Therefore, the in-plane and out-of-plane yield functions are assumed to be functions of pure in-plane and out-of-plane stress components, respectively. The in-plane model incorporates nonlinear kinematic and isotropic hardening to capture the anisotropic hardening effect. The multi-surface based in-plane yield criterion is

$$\Phi_{inp}(\mathbf{M},\boldsymbol{\chi},R)=\left\{\sum_{\alpha=1}^{6}\left\{x_\alpha\left[\frac{(\mathbf{M}-\boldsymbol{\chi}):\mathbf{M}^\alpha}{r_\alpha^0}\right]^{2k_1}\right\}\right\}^{\frac{1}{2k_1}}-(\sigma_0+R), \tag{6}$$

where $\mathbf{M}$ and $\boldsymbol{\chi}$ are the Mandel stress tensor and the back stress tensor, respecitvely, and x_α is a switch to determine whether the current stress activates the αth yield plane and is defined as

$$x_\alpha=\begin{cases}1 & \text{if } (\mathbf{M}-\boldsymbol{\chi}):\mathbf{M}^\alpha>0,\\ 0 & \text{otherwise.}\end{cases} \tag{7}$$

k_1 is an integer to smooth the corners between adjacent sub-surfaces, which is taken to be greater than 1. The constants σ_0 and r_α^0 in (6) denote the reference initial yield stress and the ratio of distance between the origin and the αth yield plane to the reference value, σ_0, respectively. Note that the use of r_α^0 enables to deal with the different yield stresses in the states of tension and compression, which results in an asymmetric yield surface. Here, a set of yield plane tensors, $\mathbf{M}^\alpha$, normal to the yield plane, are introduced as

$$\mathbf{M}^\alpha=N_{11}^\alpha\mathbf{M}_1+N_{22}^\alpha\mathbf{M}_2+N_{12}^\alpha(\mathbf{N}_1\otimes\mathbf{N}_2+\mathbf{N}_2\otimes N\mathbf{N}_1), \tag{8}$$

where N_{11}^α, N_{22}^α and $N_{12}^\alpha$are constants fitted from experiments.

The out-of-plane yield criterion bounds the standard Drucker-Prager yield surface with two surfaces perpendicular to the normal axis so as to consider the pressure dependence. In order to construct the yield function, it is helpful to incorporate the relative stress tensor into a normal-shear stress vector,

$$\mathbf{T}=[\mathbf{M}:\mathbf{M}_3,\sqrt{\mathbf{M}:\mathcal{A}\mathbf{M}}]^T, \tag{9}$$

where the fourth-order tensor $\mathcal{A}$ characterizes the plastic anisotropy in different out-of-plane shear directions. By analogy with the in-plane yield criterion (6), the following yield function is proposed by assembling three sub-surfaces, i.e. tension, compression, and shear

$$\Phi_{oup}(\mathbf{M},\boldsymbol{\sigma}_y)=\sum_{\alpha=1}^{3}\left(\frac{\langle\mathbf{T}\cdot\mathbf{H}^\alpha\rangle}{\sigma_{y\alpha}}\right)^{2k_2}-1, \tag{10}$$

where k_2 is an integer to smooth the corners between adjacent sub-surfaces, which is taken to be greater than 1. The Macaulay bracket, $\langle\cdot\rangle$, determines whether the current stress activates the αth yield plane.

A graphical representation of the yield surfaces is illustrated in Fig. 1. Also shown is the effect of the parameters k_1 and k_2 in controlling the shape of the yield surfaces. With the increase of k_1 and k_2, the corner between adjacent sub-surfaces becomes sharper and sharper.

Using an exponential map algorithm, the constitutive model described above was implemented in the commercial finite element software Abaqus using the UMAT subroutine.

To calibrate the proposed model, five uniaxial tests were used for the in-plane part, i.e. tensile tests in the MD, CD and 45 ° directions and compression tests in the MD and CD directions. In addition, another three kinds of tests were conducted for the out-of-plane calibration: ZD tension, ZD compression, and combined compression-shear.

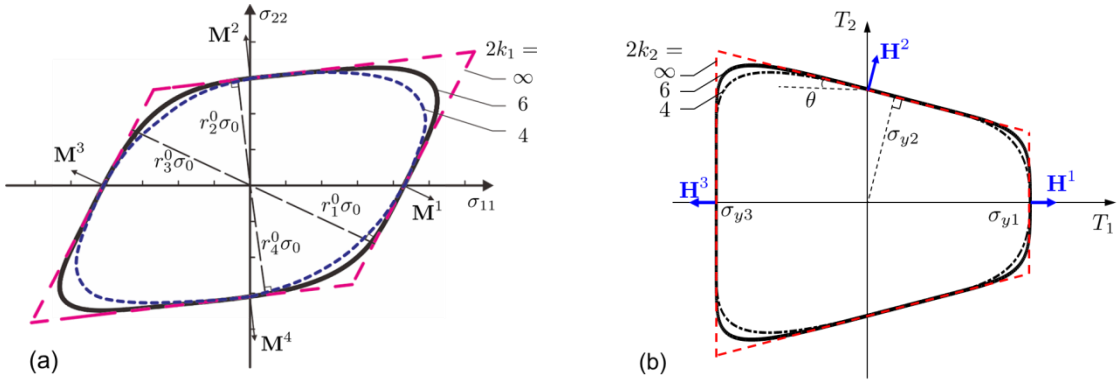

Figure 1. (a) In-plane yield surface for the biaxial loading state and (b) out-of-plane yield surface in normal-shear stress space.

Using an exponential map algorithm, the constitutive model described above was implemented in the commercial finite element software Abaqus using the UMAT subroutine.

To calibrate the proposed model, five uniaxial tests were used for the in-plane part, i.e. tensile tests in the MD, CD and 45 ° directions and compression tests in the MD and CD directions. In addition, another three kinds of tests were conducted for the out-of-plane calibration: ZD tension, ZD compression, and combined compression-shear.

For validation, experimental investigations of paper under complex loading conditions were performed. Due to the small thickness of paper, the bending stiffness is so small that it can be neglected without any significant errors. Therefore, a punch test is very suitable to evaluate the in-plane deformation behavior, with the setup shown in Figure 2(a). The whole punch test was also analyzed using the static implicit solver of Abaqus. The experimentally obtained punch force-displacement curve is compared to the numerical prediction, as shown in Figure 2(b). It indicates a good agreement between simulation and experiment (Li et al. [4]).

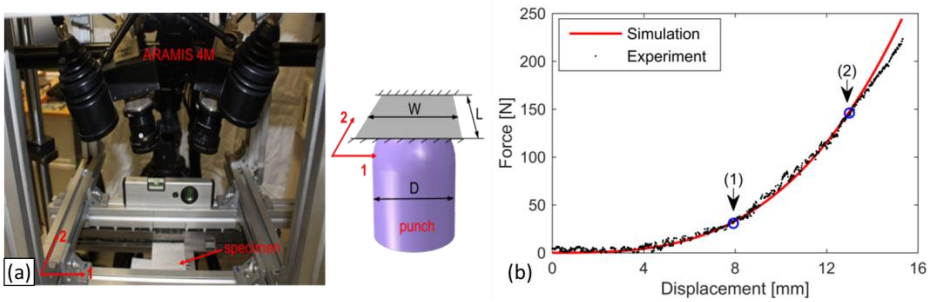

Figure 2. (a) Punch test setup and (b) force-displacement curves of the punch for both experiment and numerical prediction.

To validate the out-of-plane part of the model, a cylinder compression test was performed with the experimental setup shown in Figure 3(a). Since it is very hard to capture the strain field on the cross section of a single paper layer, a stack of paper sheets was glued together for testing. The current tests, therefore, become very suitable to verify materials models for further carton creasing investigation. Figure 3(b) shows the experimentally and numerically obtained cylinder force-displacement curves. A good match has been achieved in both loading and reloading paths.

For further validation, for both tests, the strain fields from the simulation were also compared with the experimental data. For this comparison, the loading levels indicated by 1 and 2 in Figure 2(b) and by 1, 2, and 3 in Figure 3(b), respectively, were chosen.

All the predictions displayed a reasonable agreement to experiments. Consequently, the numerical examples showed that the current model was suitable to simulate the anisotropic deformation of paper.

This will enable the simulation of complex loading conditions, such as the paperboard creasing and folding process.

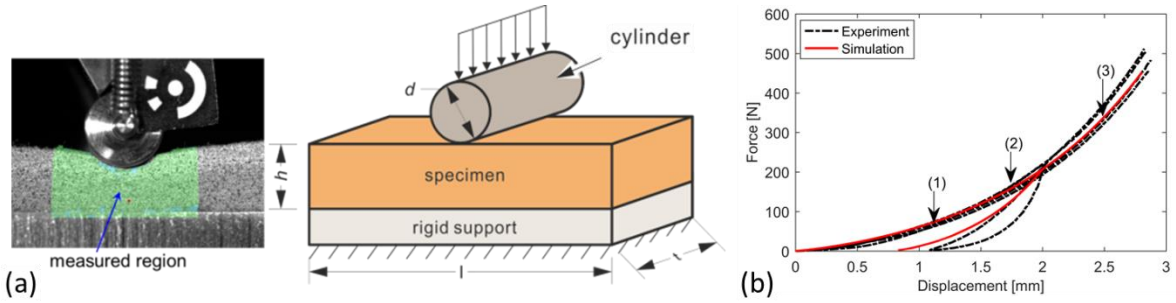

Figure 3. (a) Cylinder compression test setup and its schematic drawing and (b) force–displacement curves for both experiment and simulation of the cylinder

3 COHESIVE ZONE MODEL OF THE PAPERBOARD INTERFACE

The aforementioned fiber bridging along the crack surfaces can be modeled by using a single layer of zero thickness CZM model along the crack plane. The cohesive element behavior is characterized by a cohesive law that defines the applied stress as a function of opening displacement. In this section, a potential based cohesive law is developed to account for the fiber bridging effect in the mixed mode scenario. The potential is given by

$$\begin{aligned}\Psi(\delta_{\mathrm{n}},\delta_{\mathrm{t}}) = \min(\mathrm{G_{IC}},\mathrm{G_{IIC}}) - \frac{1}{\min(\mathrm{G_{IC}},\mathrm{G_{IIC}})} \\ \times\left[-\frac{\sigma_{\max}}{a}\left(\frac{\mathrm{e}}{a\delta_{\mathrm{nc}}}\right)^{a\delta_{\mathrm{nc}}}\Gamma(a\delta_{\mathrm{nc}}+1,a\delta_{\mathrm{n}}) + \mathrm{G_{IC}} - \min(\mathrm{G_{IC}},\mathrm{G_{IIC}})\right] \\ \times\left[-\frac{\tau_{\max}}{b}\left(\frac{\mathrm{e}}{b\delta_{\mathrm{tc}}}\right)^{b\delta_{\mathrm{tc}}}\Gamma(b\delta_{\mathrm{tc}}+1,b|\delta_{\mathrm{t}}|) + \mathrm{G_{IIC}} - \min(\mathrm{G_{IC}},\mathrm{G_{IIC}})\right],\end{aligned} \tag{11}$$

where δ_{n} and δ_{t} are the normal and tangential opening displacements along the cohesive zone, respectively, and δ_{nc} and δ_{tc} are the critical opening displacements at maximum tractions, $\sigma_{\max}$ and $\tau_{\max}$, in the normal and tangential directions, respectively. Additionally, a an b are model parameters that can be expressed in terms of the energy release rates $\mathrm{G_{IC}}$ and $\mathrm{G_{IIC}}$, respectively, which are represented by the area under the $T_n-\delta_{\mathrm{n}}$ and $T_t-\delta_{\mathrm{t}}$ curves, respectively. They are determined by solving the following equations:

$$\begin{aligned}\mathrm{G_{IC}} &= \int_0^{\infty} T_n(\delta_n)\mathrm{d}\delta_n = \frac{\sigma_{\max}}{a}\left(\frac{\mathrm{e}}{a\delta_{\mathrm{nc}}}\right)^{a\delta_{\mathrm{nc}}}\Gamma(a\delta_{\mathrm{nc}}+1,0), \\ \mathrm{G_{IIC}} &= \int_0^{\infty} T_t(\delta_t)\mathrm{d}\delta_t = \frac{\tau_{\max}}{b}\left(\frac{\mathrm{e}}{b\delta_{\mathrm{tc}}}\right)^{b\delta_{\mathrm{tc}}}\Gamma(b\delta_{\mathrm{tc}}+1,0),\end{aligned} \tag{12}$$

where the incomplete gamma function, $\Gamma(x,y)$, is introduced as:

$$\Gamma(x,y) = \int_y^{\infty} t^{x-1}\exp(-t)\,\mathrm{d}t. \tag{13}$$

It is a coupled potential based mixed mode criterion and includes six independent material parameters. By taking the derivative of the above potential with respect to δ_{n} and δ_{t}, respectively, the corresponding tractions are obtained as following:

$$\begin{aligned}T_n(\delta_n,\delta_t) = \frac{\partial\Psi(\delta_n,\delta_t)}{\partial\delta_n} = \frac{1}{\min(\mathrm{G_{IC}},\mathrm{G_{IIC}})}\left[\sigma_{\max}\left(\frac{e\delta_n}{\delta_{nc}}\right)^{a\delta_{nc}}\exp(-a\delta_n)\right] \\ \times\left[\frac{\tau_{\max}}{b}\left(\frac{e}{b\delta_{tc}}\right)^{b\delta_{tc}}\Gamma(b\delta_{tc}+1,b|\delta_t|) - \mathrm{G_{IIC}} + \min(\mathrm{G_{IC}},\mathrm{G_{IIC}})\right.\end{aligned} \tag{14}$$

and

$$T_t(\delta_n,\delta_t)=\frac{\partial\Psi(\delta_n,\delta_t)}{\partial\delta_t}=\frac{1}{\min(\mathrm{G_{IC}},\mathrm{G_{IIC}})}\left[\tau_{\max}\left(\frac{\mathrm{e}|\delta_t|}{\delta_{tc}}\right)^{b\delta_{tc}}\exp(-b|\delta_t|)\right]\frac{|\delta_t|}{\delta_t}$$
$$\times\left[\frac{\sigma_{\max}}{a}\left(\frac{\mathrm{e}}{a\delta_{nc}}\right)^{a\delta_{nc}}\Gamma(a\delta_{nc}+1,a\delta_n)-\mathrm{G_{IC}}+\min(\mathrm{G_{IC}},\mathrm{G_{IIC}})\right] \tag{15}$$

The potential together with the representative traction-separation relations in the normal and tangential directions are plotted in Fig. 4.

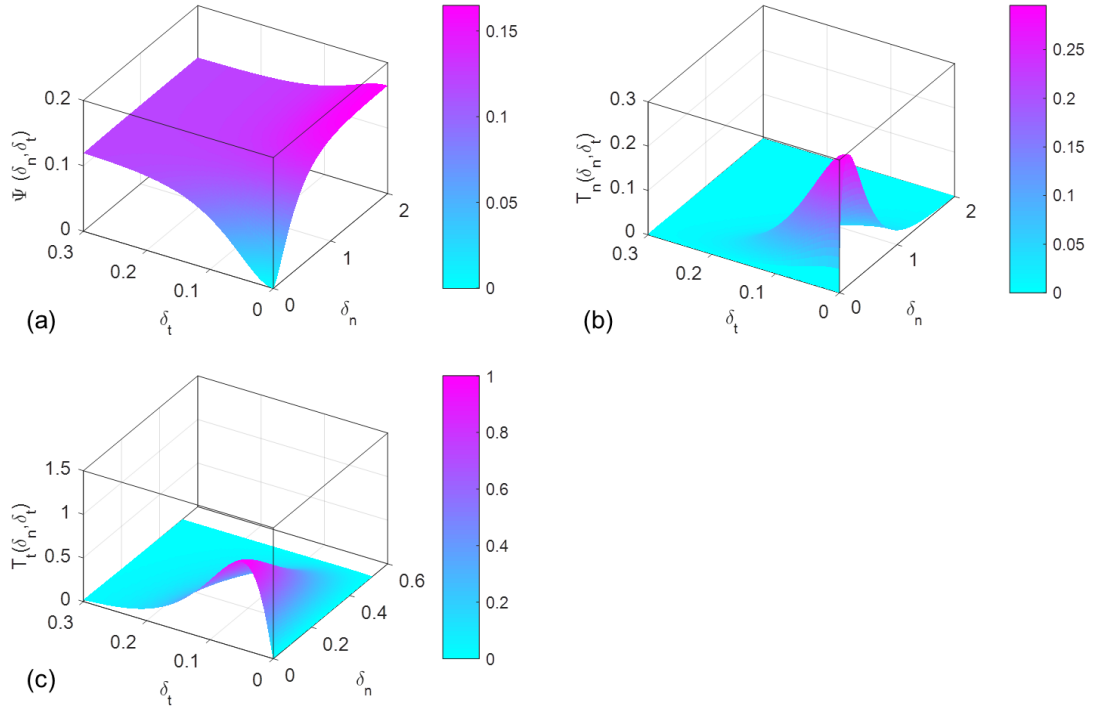

Figure 4. (a) Potential, (b) normal traction-separation relation and (c) tangential traction-separation relation for the cohesive model with $\mathrm{G_{IC}}=0.115$ MPa·mm, $\mathrm{G_{IIC}}=0.075$ MPa·mm, $\sigma_{\max}=0.295$ MPa, $\tau_{\max}=1.03$ MPa, $\delta_{nc}=0.1$ mm, and $\delta_{tc}=0.03$ mm.

4 PAPERBOARD CREASING

To simulate the creasing of the paperboard, a three-dimensional finite element model was built, which is schematically represented in Fig. 5. The paperboard examined in this paper consists of five fiber plies. At both ends of the system, blank holders ensured that the laminate was creased appropriately while the punch was moved downwards. Symmetry conditions were applied. All tools were considered rigid, whereas the paperboard was equipped with the elastic-plastic material model described in the previous section. The contact between paperboard and tools was assumed frictionless. As shown in Fig.5, the significant delamination was observed after creasing.

5 CONCLUSIONS

The current work presents a framework to model the highly anisotropic and nonlinear mechanical behavior of paper sheet and the interface delamination phenomenon. The proposed elastic-plastic model and the CZM model have been used to simulate the paperboard creasing process. One of the major areas of future work is to include the visco effect, especially in the extremely high loading speed range which usually occurs in practical creasing and folding processes. Additionally, the combined effects of moisture and temperature on the mechanical response of paper sheet and paperboard interface are important aspects for packaging products as well.

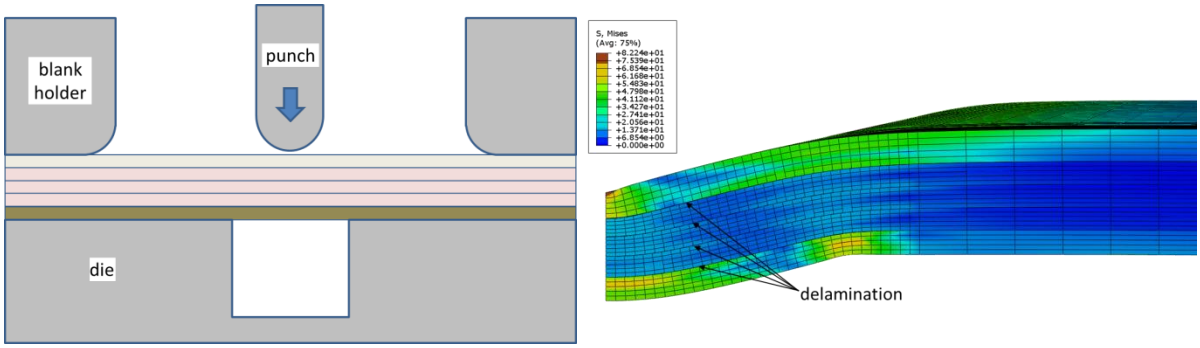

Figure 5. Schematic representation of the finite element model and the simulation results

ACKNOWLEDGEMENTS

The first author gratefully acknowledges the financial support of the China Scholarship Council (CSC). The last author is grateful for financial support of the Ministry of Innovation, Science and Research of the State of North Rhine-Westphalia, Germany.

REFERENCES

[1] Stenberg, N. A model for the through- thickness elastic-plastic behaviour of paper. *International Journal of Solids and Structures.* Vol. **40**(26): 7483-7498, 2003.

[2] Xia, Q. X. S., et al. A constitutive model for the anisotropic elastic-plastic deformation of paper and paperboard. *International Journal of Solids and Structures*, Vol. **39**(15): 4053-4071, 2002.

[3] Li, Y., S. E. Stapleton, S. Reese and J.-W. Simon. Anisotropic elastic-plastic deformation of paper: In-plane model. *International Journal of Solids and Structures.* Vol. **100**: 286-296, 2016.

[4] Li, Y., S. E. Stapleton, J.-W. Simon and S. Reese (2016). "Experimental and Numerical Study of Paperboard Interface Properties." *Experimental Mechanics*. Vol. **56**(8): 1477-1488..

[5] Fellers, C., S. Ostlund and P. Makela (2012). "Evaluation of the Scott bond test method." Nordic Pulp & Paper Research Journal **27**(2): 231-236.

[6] Korin, C., M. Lestelius, J. Tryding and N. Hallback (2007). "Y-peel characterization of adhesively-bonded carton board: an objective method." *Journal of Adhesion Science and Technology*. Vol. **21**(2): 197-210.

[7] Reese, S., T. Raible and P. Wriggers. Finite element modelling of orthotropic material behaviour in pneumatic membranes. *International Journal of Solids and Structures*. Vol. **38**(52): 9525-9544, 2001.